

OPEN ACCESS

## Elucidating Nucleation Stages of Transgranular Stress Corrosion Cracking in Austenitic Stainless Steel by In Situ Electrochemical and Optical Methods

To cite this article: Helmuth Sarmiento Klapper *et al* 2019 *J. Electrochem. Soc.* **166** C3326

View the [article online](#) for updates and enhancements.

### You may also like

- [Stress corrosion cracking and fracture behaviors of gaseous-hydrogenated Titanium alloy Ti-6321 during slow strain rate tests](#)  
Yali Xu, Longteng Li, Yanchao Yin et al.
- [Enhanced stress corrosion cracking resistance and electrical conductivity of a T761 treated Al-Zn-Mg-Cu alloy thin plate](#)  
Xu Chen, Sudan Zhai, Di Gao et al.
- [Review—Factors Influencing Sulfur Induced Corrosion on the Secondary Side in Pressurized Water Reactors \(PWRs\)](#)  
Da-Hai Xia, Yashar Behnamian and Jing-Li Luo



245th ECS Meeting • May 26-30, 2024 • San Francisco, CA

Present your work at the leading electrochemistry & solid-state science conference.

Network with academic, government, and industry influencers!

Submit abstracts by December 1, 2023

[Learn more & submit!](#)





## Elucidating Nucleation Stages of Transgranular Stress Corrosion Cracking in Austenitic Stainless Steel by In Situ Electrochemical and Optical Methods

Helmuth Sarmiento Klapper,<sup>1,z</sup> Bojan Zajec,<sup>2</sup> Andreas Heyn,<sup>3</sup> and Andraž Legat<sup>2</sup>

<sup>1</sup>Baker Hughes, a GE Company, Celle 29221, Germany

<sup>2</sup>Slovenian National Building and Civil Engineering Institute, SI 1000 Ljubljana, Slovenia

<sup>3</sup>Otto-von-Guericke University Magdeburg, Magdeburg 39106, Germany

The pitting and environmentally assisted cracking resistance of austenitic stainless steels (SS) is challenged in several industrial applications particularly those involving hot chloride-concentrated streams. Directional drilling used in the oil and gas exploration is one of these applications. Indeed, high strength CrMn-SS commonly used in drilling technology have a high tendency to fail by stress corrosion cracking (SCC) preceded by localized corrosion once subjected to highly chloride-concentrated drilling fluids at elevated temperatures. A comprehensive understanding regarding the mechanisms governing the transition from pitting into SCC is not currently available, though. Therefore, mechanistic aspects such as the effect of loading conditions on pit nucleation and repassivation as well as the synergistic effect between pit stabilization and the nucleation of a stress corrosion crack are of great practical significance. To investigate this an electrochemical-, optical- and mechanical- monitored SCC test was conducted on a CrMn-SS in an alkaline brine at elevated temperature. The transition from metastable to stable pitting and subsequently to SCC in this system was documented in-situ for the first time. Results supported H.S. Isaacs postulates regarding the interpretation of electrochemical signals and demonstrated that loading conditions affect pit nucleation and repassivation leading to a higher susceptibility of the material to pitting, which preceded SCC.

© The Author(s) 2019. Published by ECS. This is an open access article distributed under the terms of the Creative Commons Attribution 4.0 License (CC BY, <http://creativecommons.org/licenses/by/4.0/>), which permits unrestricted reuse of the work in any medium, provided the original work is properly cited. [DOI: 10.1149/2.0411911jes]



Manuscript submitted March 25, 2019; revised manuscript received May 13, 2019. Published May 31, 2019. *This paper is part of the JES Focus Issue on Advanced Techniques in Corrosion Science in Memory of Hugh Isaacs.*

Several industrial applications involve high chloride containing streams at elevated temperatures, which challenge the localized corrosion resistance of passive materials including austenitic stainless steels. The passivity of stainless steels might be compromised in these environments leading to pit nucleation under these conditions, and in the presence of tensile stresses, pits might further propagate in form of cracks by stress corrosion cracking (SCC).<sup>1</sup> Consequently, pitting corrosion and SCC susceptibility are not only reject criteria during design stages for materials selection in these applications; but later on, they might become a significant limiting factor to the service life of equipment manufactured using stainless steels. The last is particularly true because service conditions tend to deviate with time from those used in the initial statement of requirements for materials selection. The considerable susceptibility of austenitic stainless steels to SCC in hot chloride-containing environments is very well known,<sup>2</sup> and the associated risk is frequently managed by the selection of materials with improved corrosion resistance, typically, Nickel (Ni)-alloys.<sup>3</sup> However, in some industrial applications the use of Ni-alloys becomes prohibitive, due to their cost effectiveness, therefore, stainless steels are preferred. In those cases, their susceptibility to SCC has to be assessed, understood and properly managed to avoid catastrophic failures.

Directional drilling for oil and gas exploration is one of these industrial applications where austenitic stainless steels have found extensive use in spite of the demanding requirements in terms of corrosion resistance.<sup>4-7</sup> Manganese (Mn)-stabilized austenitic stainless steels are typically used in state-of-the-art drilling technology because of their excellent mechanical properties after strain-hardening, and the completely non-magnetic character of their microstructure, even in this condition. However, when subjected to chloride (Cl<sup>-</sup>)-containing environments at elevated temperatures, which are not uncommon in drilling operations, CrMn-stainless steels might become prone to localized corrosion.<sup>5,6</sup> Their pitting susceptibility has been demonstrated being very dependent of environmental conditions such as temperature, chloride content and pH.<sup>6</sup> In addition, when simultaneously subjected to tensile stresses these materials are also prone to

SCC. SCC is, indeed, one of the most common causes of failure in drilling equipment manufactured using CrMn-stainless steels.<sup>4,7</sup> SCC cracks, mainly transgranular, have been seen in the majority of these events being related to the occurrence of localized corrosion or taking place at conditions where localized corrosion is expected to occur in CrMn-stainless steels.

Because of its tremendous practical application, the mechanism behind the transition from passive layer breakdown into propagation by localized corrosion and/or by cracking in austenitic stainless steels has fascinated several generations of scientists, and Hugh S. Isaacs was not the exception. His pioneering work using in situ electrochemical scanning techniques with very good spatial and time resolution contributed significantly to elucidate the early stages of pitting corrosion on stainless steels.<sup>8,9</sup> Isaacs was the first that highlighted, based on these experimental results, the crucial role of passive layer properties in the pit stabilization.<sup>8</sup> According to Isaacs, these properties affect how the acidified highly chloride-concentrated environment inside the pit is confined, keeping it in permanent contact with the actively dissolving surface. This active dissolution inside the pit undermines the surface and led to the formation of a pit cover, which also prevents repassivation by keeping the metal-chloride concentration unaffectedly high.<sup>9</sup> Isaacs and coworkers also provided a deep insight into the processes governing pit growth, particularly on the competition between diffusional processes and surface reactions, which determine the metal-chloride concentration within the pit that is an essential part of the autocatalytic mechanism of pitting.<sup>9-12</sup> Indeed, Isaacs and co-workers were the first in conducting in situ X-ray absorption spectroscopy measurements to characterize the chemical speciation of the metal-chloride layer formed in pits of stainless steel.<sup>13</sup> To investigate conditions leading to the stabilization of pit growth Isaacs was also a pioneer in the application of electrochemical measurements at open circuit conditions,<sup>14</sup> and made significant contributions in the interpretation of these electrochemical signals produced during localized corrosion.<sup>15</sup> The present research work is devoted to document the transition from pitting into SCC that occurs in a CrMn-stainless steel when exposed to a chloride containing environment at elevated temperature combining in situ

<sup>z</sup>E-mail: [helmuth.sarmiento-klapper@bakerhughes.com](mailto:helmuth.sarmiento-klapper@bakerhughes.com)

electrochemical and optical methods. The obtained experimental results demonstrates, indeed, that most of Isaacs postulates are still valid today.

### Experimental

**Material and test solution.**—The susceptibility to pitting corrosion preceding the formation of stress corrosion cracks was investigated using an austenitic stainless steel having 15.1 wt% Cr, 14.9 wt% Mn, 2.4 wt% Ni, 2.1 wt% Mo and 0.4 wt% N. The material was in strain-hardened condition obtained by cold working. The yield strength and the elongation at fracture determined by tensile testing according to ASTM A370<sup>16</sup> at room temperature ( $RT = 22 \pm 2^\circ\text{C}$ ) were 995 MPa and 25%, respectively. The test environment for assessing the corrosion behavior of the investigated CrMn-stainless steel was in all cases a NaCl solution with a  $\text{Cl}^-$  concentration of 2.25 M (79.8 g/L  $\text{Cl}^-$ ). The pH of the test solution was adjusted to 8.6 at room temperature using  $\text{Na}_2\text{B}_4\text{O}_7 \cdot 10\text{H}_2\text{O}$  and NaOH, creating a buffer solution of pH 8 at  $85 \pm 2^\circ\text{C}$ . This pH was selected to simulate alkaline conditions typical in water-based drilling fluids.<sup>5</sup>

**Pitting susceptibility assessment.**—Electrochemical methods including cyclic potentiodynamic polarization tests and electrochemical noise (EN) measurements at open circuit conditions were used to assess the pitting corrosion resistance of the investigated CrMn-stainless steel. L-shaped specimens having a measuring surface area of ca. 845 mm<sup>2</sup> were taken by wire electrical discharge machining (EDM) from rod material. Before testing, the surface of the specimens was prepared by mechanical grinding up to 600 grit. Immediately after surface preparation the specimens were immersed in the test solution that was previously heated to  $85 \pm 2^\circ\text{C}$  using a thermostat.

A conventional three-electrode configuration including a Ag/AgCl/Sat.KCl reference electrode ( $+199 \text{ mV}_{\text{SHE}}$ ) and a TiO-covered Ti counter electrode was used for conducting the cyclic potentiodynamic polarization tests. The reference electrode was connected to the test solution via a salt bridge while the actual reference electrode element was located outside of the double-walled corrosion cell at room temperature. Prior to the start of the polarization scan, the open circuit potential (OCP) was monitored for one hour. The potential scan started at a potential that was 100 mV more negative than the OCP in the anodic direction using a scan rate of 0.2 mV/s. The direction of the polarization scan was switched in the cathodic direction when the current density reached  $100 \mu\text{A}/\text{cm}^2$  to characterize the repassivation behavior of the material. The cyclic potentiodynamic polarization tests were conducted using a CompactStat potentiostat manufactured by IVIUM Technologies in the Netherlands. To assess the standard deviation of the electrochemical parameters obtained from the OCP and the potentiodynamic polarization scans the test was repeated five times in separate experiments.

To collect additional information regarding pit nucleation and propagation time, which cannot be produced by the potentiodynamic polarization tests, also EN measurements at open circuit potential conditions were conducted. A three-electrode arrangement that included two (theoretically) identical working electrodes having the same specimen geometry as for the potentiodynamic test, and a Ag/AgCl/Sat.KCl reference electrode, was used for the EN measurements. The specimens were prepared by mechanically grinding to 600 grit prior to exposure to the testing solution at RT. After 2 h in the solution at RT, the temperature was increased to  $85^\circ\text{C}$  in a double-walled corrosion cell. A thermostat was used to heat the solution at a rate of 20 K/h. Then the temperature of the solution was maintained at  $83 \pm 2^\circ\text{C}$  for additional 3 to 6 h. During both steps, all the electrochemical signals were continuously recorded by a high-impedance voltmeter and a zero-resistance ammeter (ZRA), and filtered with 1 and 10 Hz low-pass filters.<sup>17</sup> The measuring device including the high-impedance voltmeter, the ZRA and the filters were manufactured by Ingenieurbuero Peter Schrems (IPS) in Germany. To record the electrochemical signals a 14-bit acquisition system was used. A frequency of 20 Hz was selected in alignment with the Nyquist-Shannon sampling theorem.

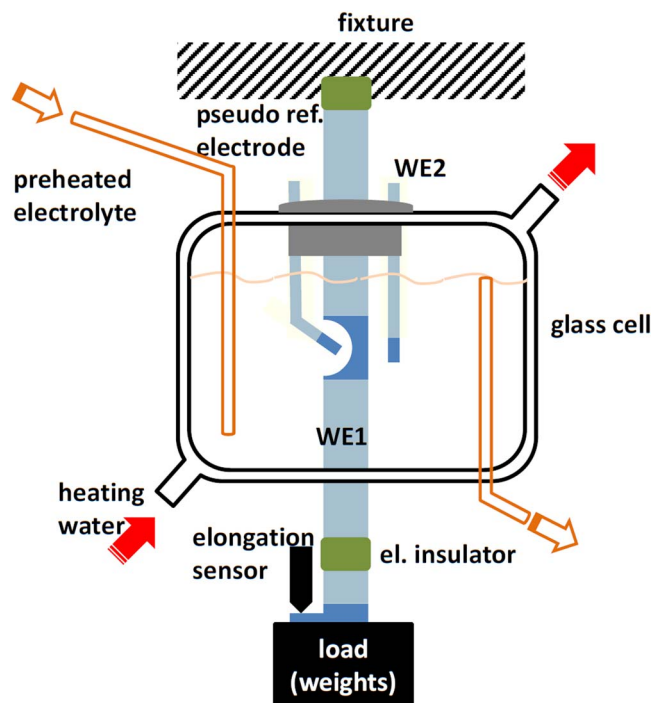


**Figure 1.** Schematics of the experimental setup. Additional elements of the electrolyte flow loop such as pump, heater and temperature sensors are not included.

**SCC testing.**—The nucleation and propagation of pits, also by SCC, was visually, mechanically and electrochemically monitored using a more advanced experimental setup similar to the one described in Reference 18.<sup>18</sup> A flat tensile specimen with dimensions of  $280 \times 12 \times 3 \text{ mm}$  was taken by wire EDM from the same batch of material. The central region of the specimen had a semi-circular notch with a radius of 9 mm at one side, where the crack is according to previous experience expected to initiate.<sup>19–20</sup> The entire gauge section was thinned by milling to a thickness of 1.1 mm leaving  $3.3 \text{ mm}^2$  as the minimal cross section of the specimen. The surface of the specimen, excluding the gauge section, was protected with a silicone coating. This enabled that the test environment, which was the same solution used for pitting susceptibility assessment, was only in contact with the gauge section ( $325 \text{ mm}^2$ ) consisting in the notched area, during the experiment. For the purpose of the EN measurements, a three-electrode configuration was used. The notched specimen subjected to a tensile stress was the primary working electrode (WE1). Additionally, two specimens manufactured from the same batch of material having a cross section of  $2 \times 3 \text{ mm}$  were positioned in the close vicinity to the gauge section of the notched specimen. One of those was located near the circumferential notch and served as pseudo-reference electrode, while the other one served as secondary working electrode (WE2). Each of them was mechanically ground with SiC paper (600 grit) and had an exposed area of  $86 \text{ mm}^2$ , making the three-electrode configuration asymmetric. This compromise was done to guarantee that the current and potential fluctuations were predominantly produced at the gauge section of the notched specimen surface, which was mechanically prepared with SiC paper (220 grit) in longitudinal direction. The whole three-electrode arrangement was enclosed in a double-walled corrosion cell containing 0.4 L of the test solution described previously. The electrolyte was kept at  $88 \pm 0.2^\circ\text{C}$  while permitting the straining of the tensile specimen. The bulk test solution was in a 5 L reservoir and circulated through a pre-heater and subsequently to the corrosion cell at a very slow flow rate (approx. 1.5 L/h) to avoid any hydrodynamic noise. A schematic representation of the experimental set-up is shown in Figure 1. Some components of the electrolyte flow loop including the pumps, heaters and temperature sensors are not shown in Figure 1

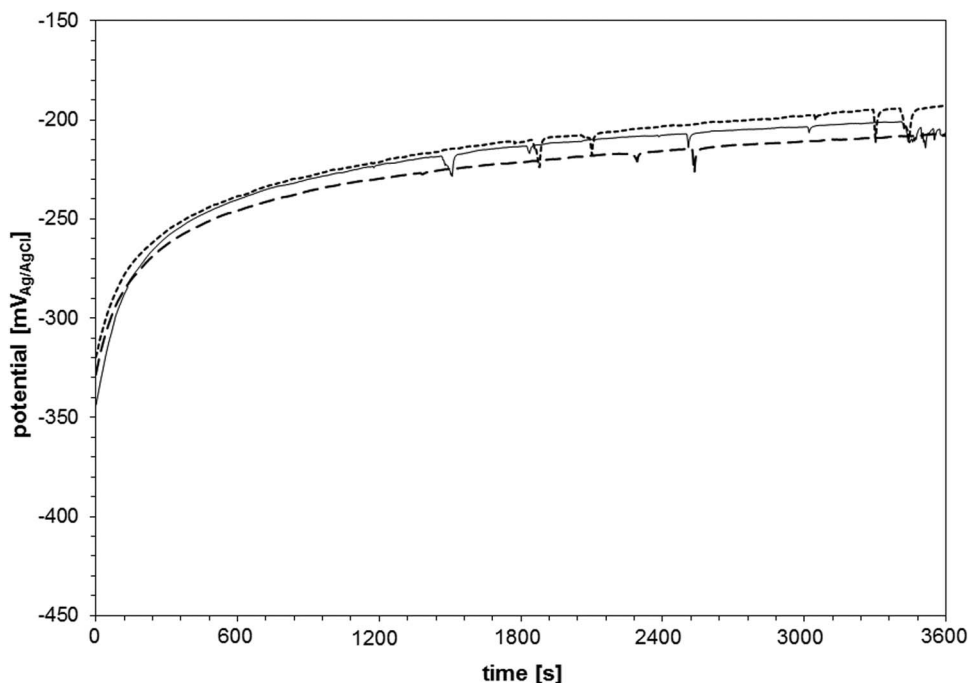


**Figure 2.** Typical OCP time records of CrMn-stainless steel in 2.25 M  $\text{Cl}^-$ -solution at 85°C.

for simplicity. The exposed areas of the three electrodes are denoted in Figure 1 by dark blue color. The notched specimen was fixed to the bottom of the glass cell using silicone sealing while flexible silicone membrane was used at the top of the glass cell to enable that the specimen elongates.

EN signals were recorded using a high-impedance voltmeter and ZRA manufactured by IPS. The polarity of the electrical connections used for the electrodes was selected in a way that a negative current flowing through the ZRA corresponds to an anodic reaction occurring at the notched specimen. The signals were filtered using a 0.8 Hz low-pass analog filter, and the corresponding sampling rate was 2 Hz. Even though the electrochemical potential of the specimen was measured using a pseudo-reference electrode, which differs from the setup used for assessing the pitting susceptibility of the investigated material, it has been decided to use the term EN to describe the electrochemical signals produced also during the SCC test. The reasoning behind is that the same phenomenon<sup>21</sup> is assessed in both experiments.

The applied tensile stress ( $\sigma$ ) was provided by weights fixed at one side of the specimen. No load control was used to avoid possible interferences with the electrochemical measurements. Nevertheless, the elongation of the tensile specimen was measured using an inductive probe with a resolution of 1  $\mu\text{m}$ . In addition, the front surface of the gauge section was imaged by a 2 mega pixel digital charge-coupled device (CCD)-camera equipped with macro photo lenses. The interval between successive images was manually set between 3 and 15 min, therefore, each image is chronologically traceable.

## Results

**Pitting susceptibility.**—Typical OCP time records of the CrMn-stainless steel in the 2.25 M  $\text{Cl}^-$ -solution are shown in Figure 2. After one hour of immersion all the tested specimens showed a similar electrochemical potential that was close to  $-210 \text{ mV}_{\text{Ag}/\text{AgCl}}$ . Metastable pitting, characterized by potential transients in cathodic direction, was observed in some of the OCP measurements. A metastable pit event comprises nucleation and time-limited growth followed by repassivation of the pit. The metastable pit events assessed in form of potential transients during the OCP measurement had typical propagation times between 20 to 60 s. In addition, the maximum amplitude of the potential transients was 25 mV. Figure 3 shows the corresponding cyclic

potentiodynamic polarization curves obtained on the CrMn-stainless steel after one hour exposure to the 2.25 M  $\text{Cl}^-$ -solution at 85°C. The average value of the OCP ( $-207 \pm 10 \text{ mV}_{\text{Ag}/\text{AgCl}}$ ) is included in Figure 3 as reference. The material remains passive in the test solution, which was confirmed by the obtained low corrosion and passive current densities. During the anodic polarization scan, however, pitting events having metastable or stable character were observed in a potential range between  $-175 \text{ mV}$  and  $-90 \text{ mV}_{\text{Ag}/\text{AgCl}}$ . After stable pit growth, repassivation occurred during the cathodic scan, at potentials more negative compared to the corrosion potential ( $E_{\text{corr}}$ ), though. The plateau observed during the reverse scan in some of the polarization curves in Figure 3 relates to the upper limit of the current range selected in the potentiostat to enable a good resolution at very low currents ( $> 1 \mu\text{A}$ ), typical in the passive range of potentials.

The pitting potential ( $E_{\text{pit}}$ ) was defined as the potential at which the current density reached  $100 \mu\text{A}/\text{cm}^2$  during the anodic polarization scan. The repassivation potential ( $E_{\text{rp}}$ ), on the other hand, was assumed as the potential at which the current density returned to  $1 \mu\text{A}/\text{cm}^2$  close to the interception between the cathodic and the anodic polarization scans. The average value and corresponding standard deviation for the  $E_{\text{pit}}$  and  $E_{\text{rp}}$  were  $-110 \pm 24 \text{ mV}_{\text{Ag}/\text{AgCl}}$  and  $-255 \pm 33 \text{ mV}_{\text{Ag}/\text{AgCl}}$ , respectively. To quantify the pitting corrosion susceptibility of the investigated stainless steel, the pitting susceptibility factor ( $PSF$ ) was calculated according to Equation 1.<sup>22</sup> The average of the OCP-value measured after one hour of exposure to the test environment, which was in good agreement with corrosion potential ( $E_{\text{corr}}$ ) determined from the potentiodynamic polarization curve ( $E_{\text{corr}} = -202 \pm 11 \text{ mV}_{\text{Ag}/\text{AgCl}}$ ), was used for calculating the  $PSF$ .

$$PSF = \frac{E_{\text{pit}} - E_{\text{rp}}}{E_{\text{pit}} - OCP} \quad [1]$$

The obtained  $PSF$ -value of  $1.52 \pm 0.43$  exceeds the susceptibility threshold<sup>22</sup> indicating that the CrMn-stainless steel is prone to pitting in the 2.25 M  $\text{Cl}^-$ -solution at 85°C. The susceptibility of the material to pitting corrosion at 85°C was confirmed in the EN-monitored exposure test. During the first 2 h at RT a similar drift in the OCP to the one observed in Figure 2, but without any electrochemical activity in potential or current, was observed. In contrast, some electrochemical activity related to metastable pitting was discerned during the heating process once the temperature of the solution was approaching to

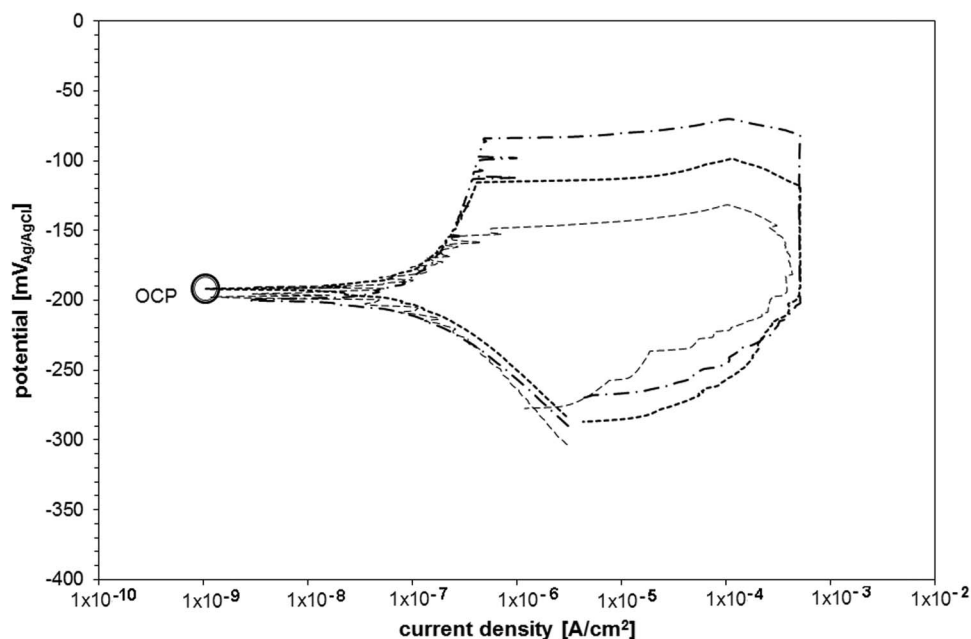


**Figure 3.** Typical cyclic polarization curves of CrMn-stainless steel in 2.25 M  $\text{Cl}^-$ -solution at 85°C.

the target value of 85°C. This activity was characterized by transients in both potential and current. Once the temperature reached 85°C, it was kept constant but the OCP continued drifting to potentials more positive than  $-175 \text{ mV}_{\text{Ag/AgCl}}$ . Figure 4 includes the time records for potential and current obtained from the CrMn-stainless steel in the 2.25 M  $\text{Cl}^-$ -solution for a period of 2 h at a constant temperature of 85°C. Only the EN signals recorded using the 1 Hz low-pass-filter are shown in Figure 4 since no additional electrochemical information was obtained using the 10 Hz low-pass filter. After approximately 15 min two metastable events occurred at one of the working electrodes. These metastable pit events had propagations times between 10 to 15 s, taken from the corresponding transients in current. Subsequently, the OCP continued drifting as previously. At an OCP-value close to  $-155 \text{ mV}_{\text{Ag/AgCl}}$ , after 25 min at 85°C, a continuous drop in the

potential as well as an increase in current were recorded. The increase in the current suggests that the electrons flowed exclusively from one specimen through the ZRA to the second working electrode. This was confirmed by post-test microscopic investigations where one single pit was found on one specimen of the CrMn-stainless steel (Figure 5). The pit grew stably for the next 95 min before the test was stopped. In a second experiment, which was reported elsewhere,<sup>23</sup> only metastable pitting was observed over an exposure time of 180 min at 85°C. Transition to stable pit growth occurred after an incubation period of 200 min and at a slightly more positive potential compared to the first experiment.

**SCC tests.**—Figure 6 shows the time records for the potential difference, current and elongation, as well as the rate of transients in

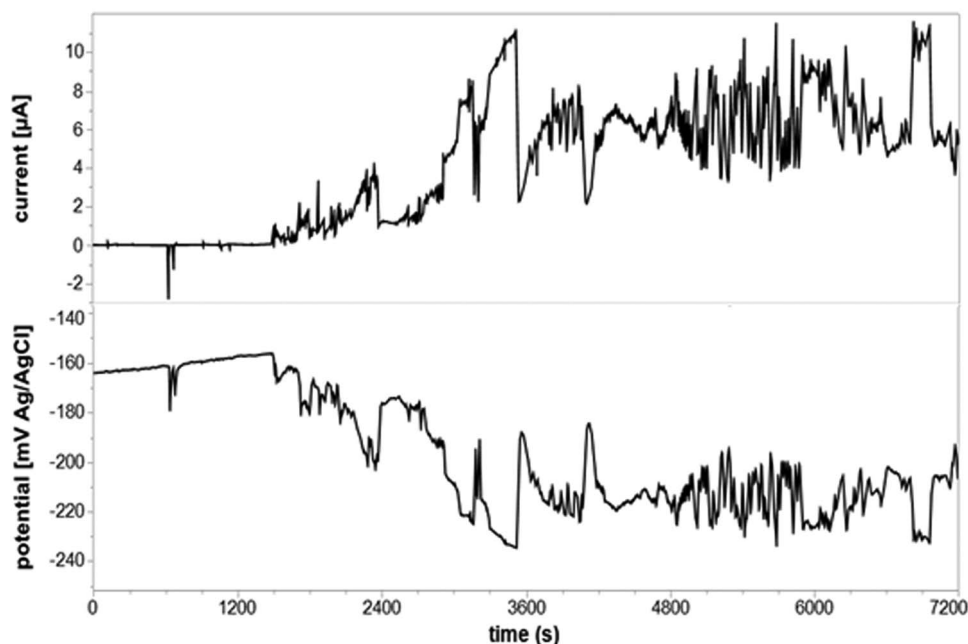


**Figure 4.** Time records of potential and current from CrMn-stainless steel in 2.25 M  $\text{Cl}^-$ -solution at 85°C.



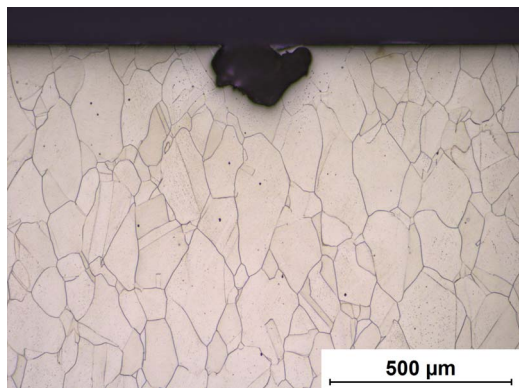


**Figure 5.** Detail of pit formed in the CrMn-stainless steel during EN-monitored exposure test in 2.25 M  $\text{Cl}^-$ -solution at 85°C.

current obtained during the experiment using the notched specimen. The potential difference corresponds to the deviation in potential between the primary working electrode (notched specimen) and the pseudo-reference electrode both manufactured using the investigated CrMn-stainless steel. For simplicity, this parameter is further referenced as potential in this manuscript. The rate of transients is calculated in 30 min intervals, where a transient is defined as an excursion of the current signal below an arbitrary threshold of  $-10$  nA and backward. As indicated previously, in the first hours no loading conditions were applied to the notched specimen. In this period of time, the potential and current signals have shown a significant amount of metastable pitting activity at the surface of the CrMn-stainless steel exposed to the 2.25 M  $\text{Cl}^-$ -containing solution at 88°C. The rate of transients related to metastable pitting decreased with time. The transients in current had typical duration times in the order of a few seconds. Figure 7 shows an extract of the time records obtained from the unloaded specimen that details the metastable activity observed in this phase of the experiment. No stable pit growth was observed after 8 h of exposure to the test environment at 88°C. Subsequently, a tensile stress of 830 MPa

at the notched-cross section was applied to the specimen. This change in the loading condition of the notched specimen is indicated by the first vertical green line in Figure 6.

Once a tensile stress of 830 MPa was applied, a slight increase in the electrochemical activity related to metastable pitting was observed. However, the rate of transients decreased with time, similar to the behavior previously observed in the first 8 h under unloaded conditions. In fact, during the last 2 h of exposure to the test solution at 88°C under a tensile stress of 830 MPa no transients could be discerned. The amplitude of the transients in potential and current increased after applying the tensile stress to the specimen, though (Figure 6). In addition, some metastable pit events have shown prolonged propagation times compared to those obtained under the unloaded condition. The optical monitoring system enabled the documentation of several metastable events including one pit that was emitting gas bubbles during the rest of the experiment (Figure 8a). This pit is further referenced in this manuscript as pit # 1 (Figure 8b). No electrochemical signals were correlated to the evolution and detachment of the bubbles produced at pit # 1.

The formation of a metastable pit was in some cases optically documented by the appearance of a small brownish spot at the imaged surface (Figure 8c), in some others by a darkish spot, between two consecutive images. Darkish spots were typically bigger in size compared to the brownish ones, but none of them increased in size afterwards. For each of these darkish spots, a current and corresponding potential transient could be discerned. One such example is presented in Figure 9 where the transients in current and potential are chronologically correlated to the formation of the brownish spot shown in Figure 8c. The transients in current and potential included in Figure 9 could be indisputably attributed to the formation of these brownish corrosion products, since this was the only event documented by the EN signals in the 15 min interval between the two consecutive images shown in Figures 8b and 8c. All such metastable pits nucleated and repassivated quickly and the transient duration in current was in the order of a few seconds. In contrast, the recovery time of the corresponding transient in potential was considerably longer, in the order of minutes. The duration time of the transient in potential was not related to pit propagation, though. The transients in potential produced

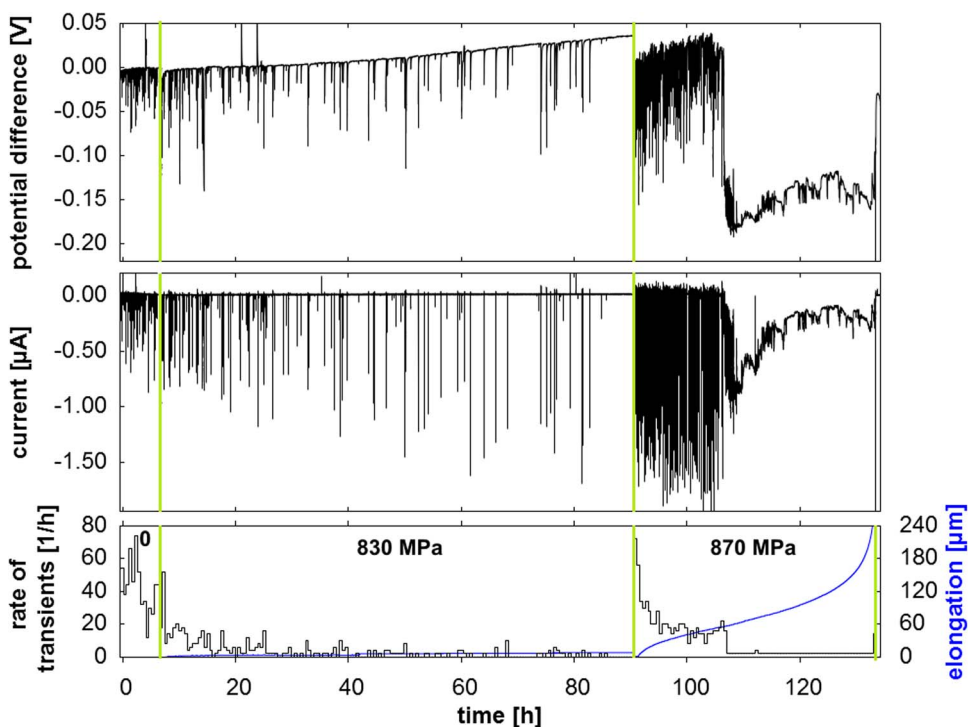


**Figure 6.** Time records of electrochemical signals arising from CrMn-stainless steel in 2.25 M  $\text{Cl}^-$ -solution at 88°C under different loading conditions.

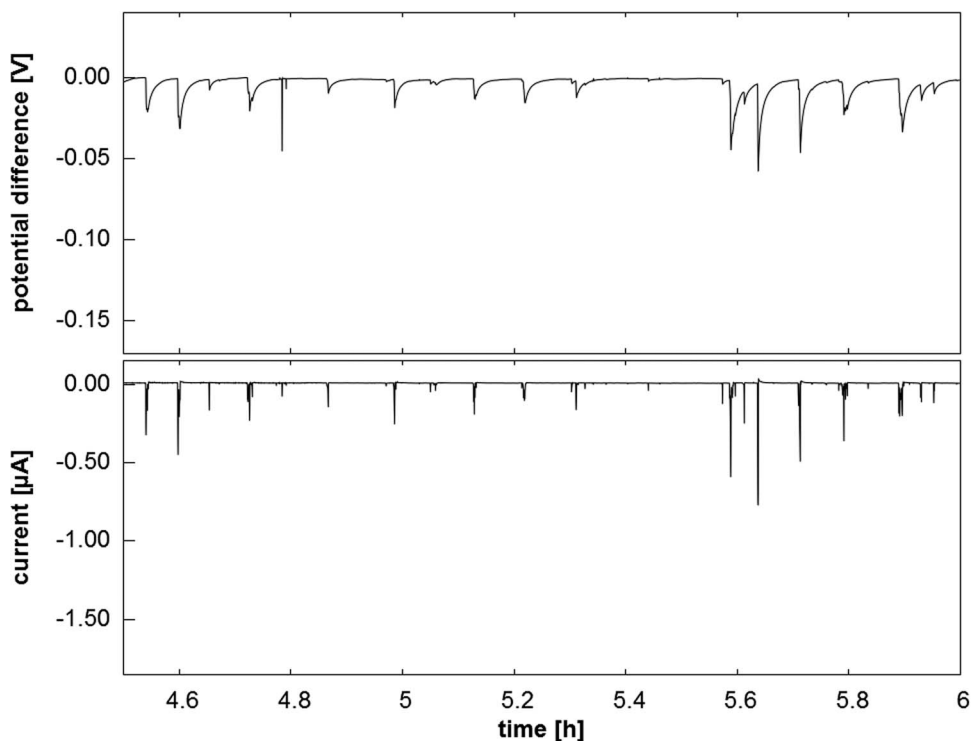


**Figure 7.** Extracts of 90 min from the time records of the EN signals obtained at unloaded conditions.

from several darkish spots where the optical images taken during the recovery time of the transient in potential were identical confirmed this. The bubble formed at pit # 1 evolved simultaneously but, as previously stated, this continuous process did not produce any change in the electrochemical signals at any time. Interestingly enough, no

correlation was observed between the location of the metastable pits, which were randomly distributed at the surface of the specimen in contact with the test environment, and the tensile stress, which is expected to be the highest at the leading edge of the notched area. In addition, during the 84 h of exposure at these experimental conditions none of the nucleated pits propagated further into a stress corrosion crack. This was further confirmed by the absence of any significant change in the elongation of the specimen (Figure 6). Therefore, the load was increased to 870 MPa. This further increase in the applied tensile stress is indicated in Figure 6 by the second vertical green line.

After the increment of the applied tensile stress to 870 MPa, a significant increase in the electrochemical activity characterized by

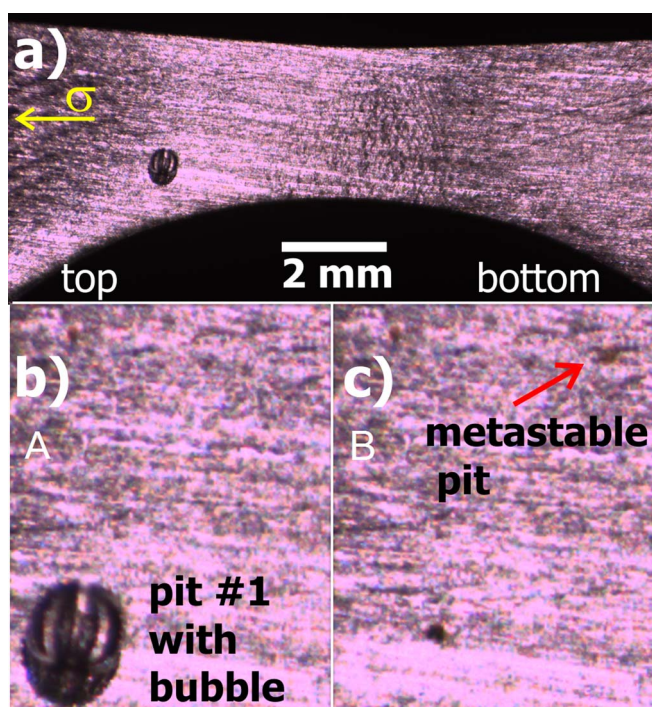


**Figure 8.** Metastable pit formed at 830 MPa: a) imaged area of the specimen with semicircular notch, b) magnified bubble formed at pit # 1, and c) subsequent bubble evolution at pit # 1 and formation of metastable pit (red arrow).

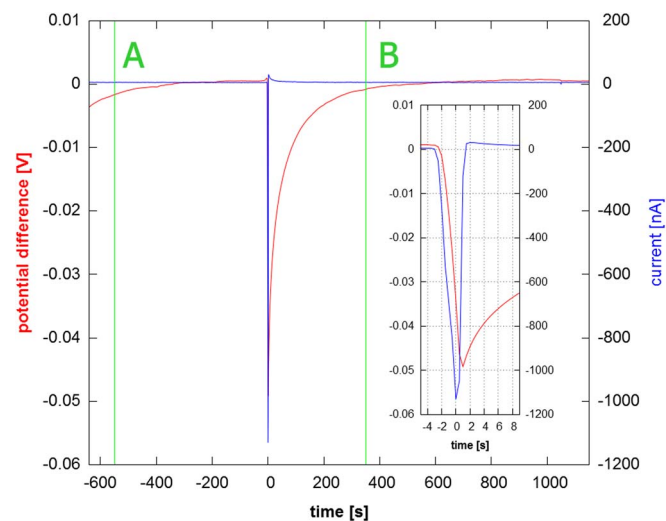


**Figure 9.** Transients in potential and current produced from metastable pit event optically documented in Figure 8c. Green vertical lines denote the imaging time. Sections of images obtained at A and B are shown in Figures 8b and 8c, respectively.



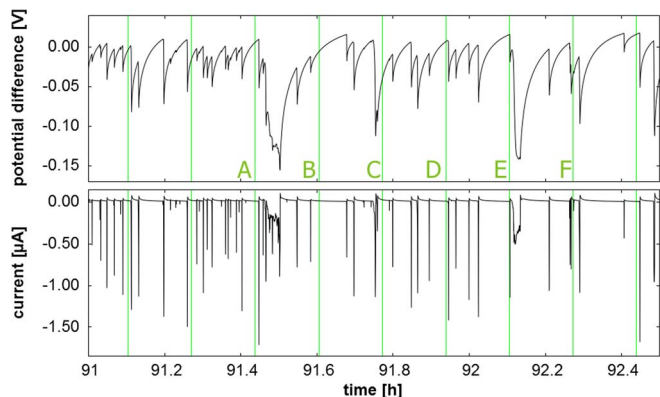


**Figure 10.** Extracts of 90 min from the time records of the EN signals and the elongation obtained right after the tensile stress was increased to 870 MPa.

a higher rate of transients, also with higher amplitudes and longer duration times was observed (Figure 10). Some of these metastable events propagated over a couple of minutes and were assessed optically as metastable pits. Figure 11 shows several images of the specimen that correlate chronologically with the electrochemical signals in Figure 10. In Figure 10 the times at which the images were captured are indicated by green lines and labeled using the same letters (A to F) as in Figure 11. It is rather difficult to highlight differences due to newly formed metastable pits from the images. Therefore, Figure 11 includes the differences between each pair of consecutive images, which were additionally enhanced using a histogram equalization filter. The transients from Figure 10 that had the longest duration times produced the most noticeable metastable pits, which are recognizable in Figures 11a (pit # 2) and 11e (pit # 3). Other transients had very short duration times and the corresponding electrochemical signals were similar to those shown in Figure 9. The corresponding surface damages are the remaining white spots in Figures 11a to 11e, that are also documented as brownish spots in Figure 11f. These brownish spots are very similar to the metastable event shown in Figure 8c. In the period between image B to F bubbles were formed and evolved from pit # 2. However, no further activity was further observed at pit # 2 afterwards. In contrast, pit # 3 was emitting bubbles after its nucleation (Figure 11e). It has to be mentioned that bubbles continued evolving

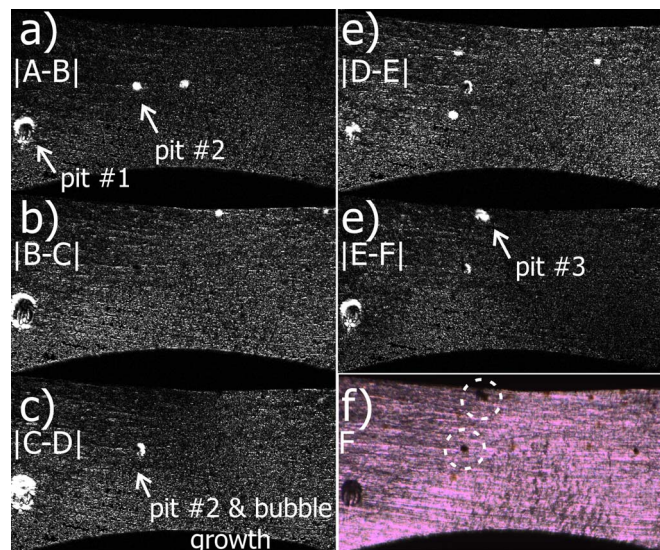


**Figure 11.** Metastable pits formed at 870 MPa including bubble formation and evolution at pit # 1. The corresponding electrochemical signals obtained between the images are indicated with green lines in Figure 10.

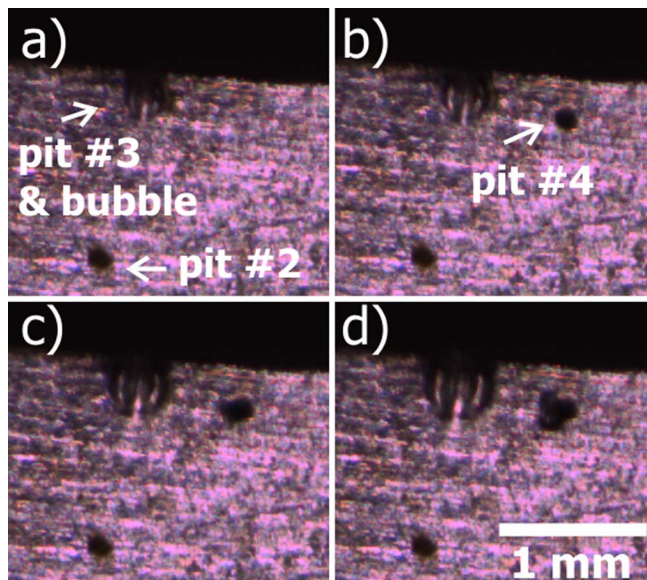


**Figure 12.** Detail of pit nucleation and propagation at 870 MPa: a) bubble formation at pit # 3, b) nucleation of pit # 4, and c) and d) growth of pit # 4 and bubble formation at pit # 3.

from pit # 1 and pit # 3 during the rest of the experiment without producing any electrochemical signal. The elongation, on the other hand, increased slowly but continuously (Figure 6).

After approximately 16 h at 870 MPa (approx. 106 h in Figure 6) a significant drop in the EN signals occurred and their appearance changed completely. From that moment, the electrochemical signals did not recover to its original value. In addition, no single transients were discerned, and the elongation increased much faster (Figure 6). Before this change in the EN signals the optical monitoring system still reported the formation and evolution of bubbles at pits # 1 and # 3 (Figure 12a), while a few minutes later, as shown in Figure 12b, pit # 4 nucleated. Bubble formation and evolution continued at pits # 1 and # 3 while pit # 4 was growing (Figures 12c and 12d). Subsequently, a bubble was also formed and evolved from pit # 4 (Figure 13a). After 1.5 h pits # 3 and 4 combined into one pit (Figures 13b and 13c), and from that moment bubbles only evolved from this combined pit as well as from pit # 1. After approximately 25 h (43 h at 870 MPa) the specimen finally failed. The time of the failure is represented in Figure 6 by the third green line in the chart that includes the elongation signal. As shown in Figure 14 the crack propagated from the pit shown in Figure 13c into the notched area. The fracture surface has shown a transgranular fracture mode beneath the pit (pits # 3 and # 4) that preceded crack formation (Figures 14a and 14b). The rest of the fracture surface was characterized by dimples indicating a ductile fracture mode. Figure 14c shows the corrosion products associated to the pit that led to the failure of the specimen as well as those from the metastable pit events. Microscopically inspection of the three electrodes confirmed that some metastable pitting also occurs at the opposite surface of the notched specimen that was not optically monitored, while no pitting damage was found on the other two electrodes used as pseudo-reference electrode and second working electrode, respectively.

## Discussion

During the EN-monitored exposure test in the 2.25 M Cl-solution of pH 8 at 85°C (Figure 4), the investigated CrMn-stainless steel has shown stable pit growth after 25 min at a potential close to the pitting potential range ( $-110 \pm 24 \text{ mV}_{\text{Ag}/\text{AgCl}}$ ) determined by the cyclic potentiodynamic polarization tests. On the other hand, the material has only shown metastable pitting during the initial 8 h of the SCC-test



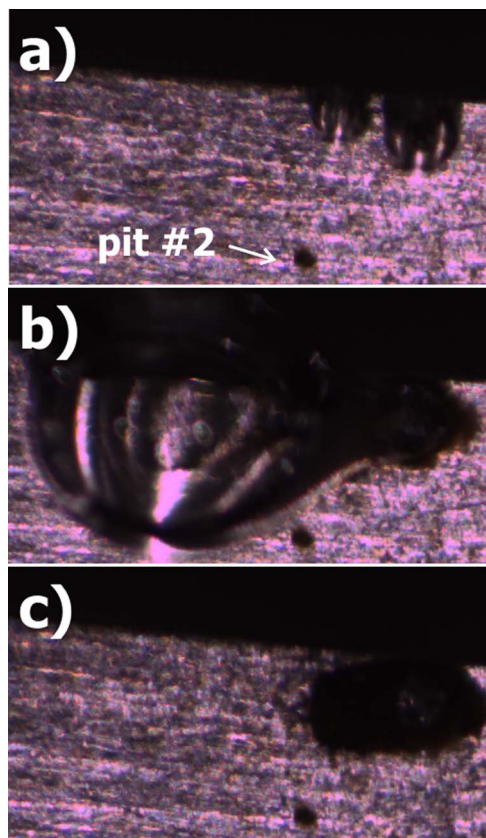


**Figure 13.** Detail of propagation process of pits # 3 and # 4: a) bubble formation at pits # 3 and 4, b) pit clustering and c) bubble evolution.

before a tensile stress was applied (Figure 6). This behavior appears to be also in contradiction with the poor repassivation ability and the corresponding *PSF*-value obtained from the polarization tests (Figure 3), which suggest the material should not be able to repassivate in the test solution once a pit nucleates. Even though the notched specimen was subjected only 8 h to the test environment without load, which does not allow to rule completely out the occurrence of stable pitting under these conditions, this discrepancy in the nucleation time can be rationalized in terms of the differences in the stabilization process of the passive layer formed on the CrMn-stainless steel. It is assumed that the passive layer existing at the surface of the notched specimen had most likely different properties compared to the one formed at the specimens used in the EN and potentiodynamic tests because all of them underwent different stabilization processes. In this regard, Isaacs et al. concluded from scanning electrochemical measurements on type 304 stainless steel having different surface conditions in 0.4 M  $\text{FeCl}_3$ -solution acidified with 0.03 M HCl to pH 0.9 that both, pit nucleation and pit propagation, depends strongly on the properties of the passive layer.<sup>8</sup> They observed that the half-lives of active pits increased with increasing the thickness of the oxide layer obtained by a thermal treatment. Isaacs explained the role of the passive layer in the propagation mechanism by confining the environment inside the pit, keeping it in contact with the actively dissolving surface, and preventing its concentration from decreasing, thus, avoiding repassivation.<sup>9</sup> While the fresh prepared specimens for the EN-monitored test, for instance, had a stabilization time of 120 min in the test solution at RT before the temperature was increased and kept at 85°C, the notched specimens was initially exposed 40 min to the solution before the temperature reached and stabilized at 88°C. A quantitative comparison of the electrochemical condition of the specimens is rather difficult because in the SCC setup a pseudo-reference electrode was used for measuring the potential difference between the primary (notched specimen) and the secondary working electrodes. Thus, a true electrochemical poten-

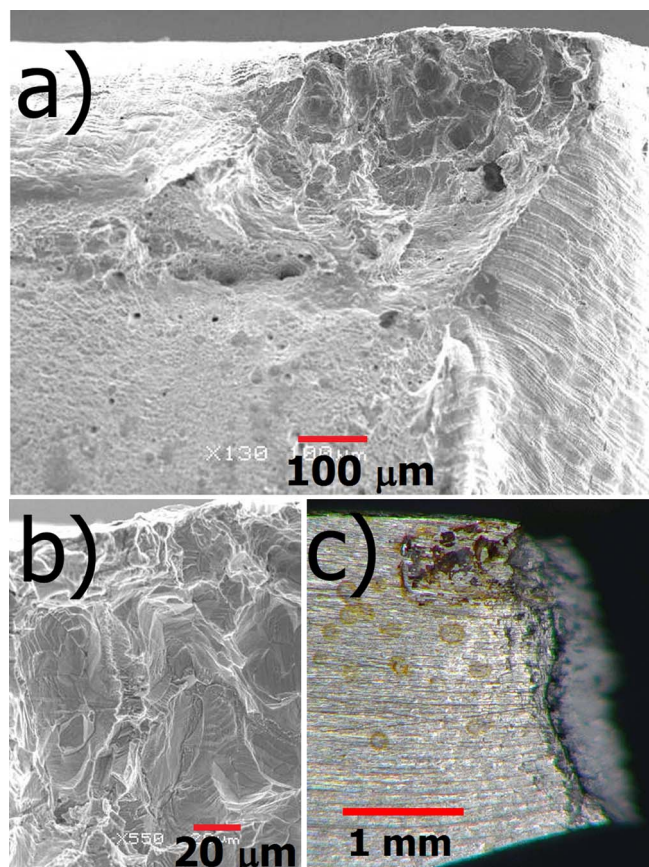


**Figure 14.** Post-test documentation of failed CrMn-stainless steel specimen subjected to different loading conditions in 2.25 M Cl<sup>-</sup>-solution at 88°C: a) and b) SEM micrographs of the initiation site, and c) optical image of the failed specimen including pitting damage.

tial cannot be established and compared to the potential measured by the Ag/AgCl/Sat.KCl reference electrode.

One can infer, nevertheless, that the electrochemical potential of the notched specimen most likely remained less positive compared to the potential range for stable pit growth determined by the potentiodynamic scan and confirmed in the EN-monitored exposure tests. Consequently, no stable pitting was obtained on the notched specimen before a tensile stress was applied. A significant difference in the OCP is expected between the notched specimen and the specimens used in the EN-monitored exposure test due to the fact that the effective area is almost five times smaller in the SCC experiment. The larger the area the more the surface available for the oxygen reduction reaction that supports a faster approximation to the critical range of potentials where stable pitting might occur. Isaacs et al. postulated that the probability of forming a stable pit in stainless steels increases with the effective area, which is not necessarily related to the probabilistic aspect of pit initiation but to the stabilization of the pit propagation after initiation. Isaacs explained that the capacitance increases with the surface area leading to a decrease in the magnitude and rate of the potential change.<sup>14</sup> Because more charge is available, the potential does not drop below a protection potential and the pit can propagate, as observed in Figure 4. It is also believed that the corrosive damage concentrated on the surface of the notched specimen because it was subjected to the loading conditions. This might have had an additional protective effect on the secondary working electrode, on which no pitting damage was observed.

Metastable pitting reproducibly occurred, on the other hand, in all three different experimental setups. During the EN-monitored exposure test, for instance, metastable pitting occurred at potentials approx. 100 mV more positive to the repassivation potential range

( $-255 \pm 33$  mV<sub>Ag/AgCl</sub>) determined by the cyclic potentiodynamic polarization scans. This suggests that  $E_{\text{tp}}$ -values obtained by polarization methods where stable pit growth is artificially controlled should be carefully used for predicting repassivation behavior in service. This limitation is also relevant for materials selection purely based on repassivation potentials assessed by these techniques. As recognized by Isaacs,<sup>9</sup> the use of EN measurements for assessing pit nucleation and growth at OCP conditions seems to be more appropriate since the kinetic of the electrochemical reactions involved into the incubation and repassivation steps are not significantly influenced. In spite of the obtained large difference in the incubation times for stable pitting, the propagation times of metastable pit events assessed in form of isolated transients during the EN measurements using two identical (L-shaped) specimens, and two dissimilar (notched and un-notched) specimens, none of them loaded, were in the same order of magnitude.

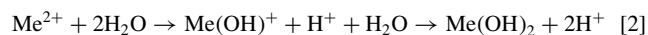
As previously mentioned, several EN transients related to metastable pitting were discerned during the different phases of the SCC experiment. While transients in current were characterized by having a rapid decrease followed by a faster recover, the corresponding transients in potential had a typical shape consisting of a rapid decrease, very similar to the one observed for the transient in current, followed by a much slower recover. According to Isaacs et al. the typical shape of potential transients arising from metastable pitting events at OCP relates to the consumption of the charge from the interfacial capacitance of the passive surface; once the pit repassivates, the capacitance is slowly recharged due to the slow cathodic reaction occurring at the passive layer.<sup>15,24</sup> Even though the sampling rate set for the optical system does not allow a complete clarification of the relation between the shape of the EN signals and the reactions involved in the pitting process, in few cases including the metastable pit event shown in Figures 8 and 9, it was established that the time necessary for the potential to recover to the initial value after a metastable pit event is not related to pit growth, which confirms Isaacs postulate.<sup>24</sup>

In spite of the fact that a tensile stress was not a pre-requisite for pit nucleation and pits did not preferentially nucleate at the notched area of the specimen where the highest tensile stress was expected to be localized, the introduction of a tensile stress led to a significant increase in the metastable pitting activity of the material. This was characterized by an increase in the frequency but especially in the amplitude of the transients as shown in Figures 6, 7 and 10. In addition, the metastable pit propagation times, taken from transients in current, increased with increasing the applied tensile stress from seconds (Figure 7) to minutes (Figure 10). This suggests that the tensile stress does not only have a detrimental effect on pit nucleation but also on the repassivation behavior of the investigated material. While the transition from metastable to stable pitting could be discerned in the electrochemical measurements crack initiation and especially crack propagation could not be distinguished electrochemically but inferred using the rapid increase in the elongation signal. Indeed, this inflection point in the elongation signal occurred between 104 and 108 h, while the transition to stable pitting occurred at 106.5 h (Figure 6). Therefore, it can be assumed that the stabilization of the pit shown in Figure 13c led immediately or a few hours later to crack initiation and propagation by SCC.

As previously described in the experimental results the co-evolution of bubbles from some pits, especially those that had prolonged propagation times, was documented with the CCD-camera (Figures 8, 11 and 13). Pit # 1, which nucleated and repassivated just before a tensile stress was applied, for instance, was emitting gas bubbles over more than 96 h at a constant rate (approx.  $8 \cdot 10^{-8}$  L/h). The reported rate was calculated by assuming a semispherical shape of the bubble while its diameter and the time between formation and detachment were obtained from the optical images. One potential source for the gas bubbles might be the air dissolved into the buffer solution since the brine was not deaerated. In addition, the double-walled corrosion cell was not completely filled with the test solution that was also constantly recirculated from the reservoir to the cell. Air solubility is expected to be considerably reduced by increasing the temperature to 88°C. Measurements conducted with an optical sensor (Hamilton

Tech) in a dedicated experiment with the same aerated buffer solution confirmed a reduction in the dissolved oxygen (DO) concentration from 7.2 mg/L at RT to 2.5 mg/L by increasing the temperature to 80°C. A possible explanation for the preferential bubble formation at pits might be a high surface tension created at these cavities leading air dissolved into the solution to accumulate there and evolve from these sites by buoyancy. However, this hypothesis cannot explain why bubble formation only occurred constantly at pit # 1, for instance, while temporarily at other pits such as pit # 2, # 3 and # 4.

A second hypothesis is the formation of hydrogen bubbles, even though, the alkaline pH of the buffer solution strongly suggest that the preferred cathodic process should be the oxygen reduction reaction. DO can be reduced on stainless steels in alkaline NaCl solutions following a four-electron pathway directly to OH<sup>-</sup>-ions, or following a two-electron pathway producing hydrogen peroxide as a by-product.<sup>25,26</sup> During pitting the oxygen reduction reaction is assumed to occur at the passive surface,<sup>1</sup> even though the passive layer considerable reduces the kinetic of this reaction.<sup>27,28</sup> On the other hand, sufficient protons from cation hydrolysis according to Equation 2 are expected to be available inside the pit.<sup>1</sup> Experimental work has confirmed in the past that the pH inside pits in stainless steel could be less or about 3<sup>29</sup>, regardless the pH of the bulk electrolyte.



Indeed, hydrogen co-evolution has been already reported by Brigham taking place on type 304 stainless steel in a ferric sulfate solution containing chloride ions under crevice conditions.<sup>30</sup> Hydrogen bubbles originated at the center of the naturally occurring crevice. It was assumed by Brigham that proton reduction occurs in the occluded cell followed by hydrogen re-oxidation at the mouth of the crevice, where hydrogen bubbles act as a chemical short-circuit also restricting the volume of the electrolyte inside the pit.<sup>31</sup> Considering the experimental facts delivered in the present research work, it can be argued, that pit # 1 was producing hydrogen bubbles as a consequence of proton reduction inside the pit, which will require that the pit further propagates to supply the charge for this cathodic reaction. However, a permanent pit growth implies that this anodic site would be the preferential flaw for exceeding the stress intensity factor at a given time, leading to crack nucleation and subsequent failure, which obviously did not occur at pit # 1.

An alternative hypothesis is that pit # 1 repassivated but continued producing hydrogen bubbles because sufficient protons were previously released by cation hydrolysis inside the pit while the electrons necessary for further proton reduction were supplied from other metastable pits that nucleated later. This alternative hypothesis also implies that the internal surface of pit # 1 acts as a cathodic area for supporting the growth of other pits, which explains why no electrochemical signals could be associated to this process. A similar phenomena of pit clustering and hydrogen co-evolution was also documented on pits # 3 and # 4 (Figure 13). A correlation between metastable pit events in stainless steels have been already proposed in the past by others.<sup>32,33</sup> Using in situ electrochemical scanning Isaacs reported that a dozen of pits nucleated simultaneously on type 304 stainless steel in ferric chloride solution at RT.<sup>8</sup> The current of each active pit increased continuously over a period of approximately 20 seconds until it repassivated. The number of active pits decreased with time and only a few remained active. Isaacs reported that this process was repetitive and the subsequent generation of pits virtually never nucleated at previously repassivated pits.<sup>9</sup> Pit # 1 was further analyzed by micro-computer tomography (CT) at a pit depth of approximately 5 μm was determined, which confirms that the pit was not propagating during the rest of the experiment under different loading conditions. As suggested by Brigham<sup>31</sup> hydrogen bubbles might exacerbate an exchange between the electrolyte inside the pit and the bulk buffer solution avoiding proton neutralization. However, bubble evolution was observed taking place over 96 h and it appears unlikely that such a large concentration of protons could be maintained over such a long period of the time



inside the pit. At the same time, acidified conditions inside the pit should prevent it from repassivation and led to further propagation. Consequently, a complete clarification of this phenomenon requires additional experimental work in completely de-aerated solution.

The experimental results obtained in this research work confirmed Isaacs postulates regarding pit nucleation and propagation as well as his contributions on the interpretation of electrochemical signals arising from those processes. They also demonstrate the significant added value of using electrochemical measurements at OCP conditions for assessing early stages of localized corrosion leading to SCC. On the other hand, the experimental results have also shown that the investigated material is prone to pitting and SCC in the simulated drilling environment at temperatures around 85°C. Loading conditions have influenced significantly the pitting susceptibility of the material, which suggests that applied and residual tensile stresses might lead to catastrophic failures on drilling equipment manufactured using CrMn-stainless if not properly limited. An additional alternative to minimize the risk of having pitting and SCC is to limit the use of these materials in this type of environment or to reduce the corrosiveness of the environment itself, for instance, by increasing the pH and/or decreasing the chloride content, as demonstrated in the past by electrochemical results.<sup>6</sup>

### Conclusions

An electrochemical monitored SCC experiment was successfully conducted to document the effect of tensile stresses on the pitting corrosion and SCC susceptibility of a strain-hardened CrMn-stainless steel in an alkaline brine at elevated temperature. The EN measurements were complemented by an optical monitoring system for documenting the damage that occurred at one side of the specimen as well as by the elongation signal.


Electrochemical results from different techniques confirmed the susceptibility of the investigated material to pitting corrosion in the alkaline brine at elevated temperature selected to simulate a typical drilling environment. A pit was indeed confirmed as the precursor site for SCC. Even though pits nucleated independently of the applied tensile stress, the introduction of loading led to a significant increase in the metastable pitting activity of the material. In addition, the propagation time of metastable pits increased significantly with increasing the magnitude of the applied tensile stress, which suggests that loading conditions have also a detrimental effect on the repassivation behavior of the investigated material. The transition from metastable to stable pitting and pit clustering could be monitored electrochemically and correlated with optical images. Crack initiation and particularly crack propagation could be only distinguished by the elongation signal, though.

Two different hypothesis are discussed for the bubbles that formed and evolved from pits that nucleated at the notched specimen without producing electrochemical signals. One hypothesis suggests that bubbles are related to the air dissolved in the buffer solution used for testing. However, this does not explain why bubbles were preferentially produced and evolve from particular pits, also involving different periods of time. A second hypothesis suggests that the observed bubbles correspond to hydrogen evolution, which contrasts with the alkaline pH of the buffer solution. In spite of the fact the protons are expected to be produced inside the nucleated pits, no relation between the volume of gas produced and the expected concentration of protons

could be established. Therefore, the clarification of this phenomenon demand further investigations.

The discussion of the results obtained in the present research work clearly confirms that Hugh S. Isaacs legacy is still valid today for the interpretation of electrochemical signals arising from localized corrosion in stainless steels.

### ORCID

Helmuth Sarmiento Klapper 

<https://orcid.org/0000-0001-5798-861X>

Bojan Zajec  <https://orcid.org/0000-0001-6170-8748>

Andreas Heyn  <https://orcid.org/0000-0002-0146-219X>

### References

1. G. S. Frankel, *J. Electrochem. Soc.*, **145**, 2186 (1998).
2. M. Speidel, *Metall. Trans.*, **12**, 779 (1981)
3. H. S. Klapper, N. S. Zadorozne, and R. B. Rebak, *Acta Metall. Sin. (English Letters)*, **30**, 296 (2017).
4. P. G. Smith, J. E. Truman, H. T. Gisborne, and G. Oakes, *J. Mater. Eng.*, **6**, 300 (1985).
5. A. L. Collins, Corrosion Resistance of Non-Magnetic Drill Collars, in *Proceedings of the NACE CORROSION Conference 2001*, paper no. 1344 (2001).
6. H. S. Klapper, J. Stevens, and G. Wiese, *Corrosion*, **69**, 1095 (2013).
7. D. S. Kopecki, Residual Stress Surface Treatments for the Bore of Nonmagnetic Drill Collars, in *Proceedings of the NACE CORROSION Conference 2010*, paper no. 10266 (2010).
8. H. S. Isaacs and G. Kissel, *J. Electrochem. Soc.*, **119**, 1628 (1972).
9. H. S. Isaacs, *Corros. Sci.*, **29**, 313 (1989).
10. H. S. Isaacs, *J. Electrochem. Soc.*, **120**, 1456 (1973).
11. J. Tester and H. Isaacs, *J. Electrochem. Soc.*, **122**, 1438 (1975).
12. R. Newman and H. Isaacs, *J. Electrochem. Soc.*, **130**, 1621 (1983).
13. H. S. Isaacs, J.-H. Cho, M. L. Rivers, and S. R. Sutton, *J. Electrochem. Soc.*, **142**, 1111 (1995).
14. H. S. Isaacs and Y. Ishikawa, *J. Electrochem. Soc.*, **132**, 1288 (1985).
15. H. S. Isaacs and A. J. Davenport, *J. Electrochem. Soc.*, **137**, 2196 (1990).
16. ASTM A370 - Standard Test Methods and Definitions for Mechanical Testing of Steel Products, (West Conshohocken, PA: *ASTM International*).
17. A. Heyn, J. Göllner, M. Bierwirth, and H. S. Klapper, Recent Applications of Electrochemical Noise for Corrosion Testing - Benefits and Restrictions, in *Proceedings of the NACE CORROSION Conference 2007*, paper no.07459 (2007).
18. J. Kovač, M. Leban, and A. Legat, *Electrochim. Acta*, **52**, 7607 (2007).
19. J. Kovač, C. Alaux, T. J. Marrow, E. Govekar, and A. Legat, *Corros. Sci.*, **52**, 2015 (2010).
20. J. Kovač, T. J. Marrow, E. Govekar, and A. Legat, *Mater. Corros.*, **63**, 664 (2012).
21. H. S. Klapper, Using Electrochemical Noise to Elucidate the Mechanisms Involved in Localized Corrosion – A Review, in *Proceedings of the NACE CORROSION Conference 2018*, paper no. 11236 (2018).
22. H. S. Klapper and R. Rebak, *Corrosion*, **76**, 666 (2017).
23. H. S. Klapper, A. Heyn, and S. Jesse, Electrochemical Methods for Assessing the Pitting Corrosion Resistance of Metallic Materials in Chloride-Containing Environments at Elevated Temperatures, in *Proceedings of the NACE CORROSION Conference 2018*, paper no. 10438 (2018).
24. H. S. Isaacs, *Corros. Sci.*, **34**, 525 (1993).
25. M. Okuyama and S. Haruyama, *Corros. Sci.*, **31**, 521 (1990).
26. S. Kapusta, Oxygen reduction on stainless steels in aerated brines, in *Proceedings of the NACE CORROSION Conference 2005*, paper no.04655 (2004).
27. N. Le Bozec, C. Compere, M. L'Her, A. Laouenan, D. Costa, and P. Marcus, *Corros. Sci.*, **43**, 765 (2001).
28. H. S. Klapper and J. Göllner, *Corros. Sci.*, **51**, 144 (2009).
29. A. Turnbull, *Corros. Sci.*, **23**, 833 (1983).
30. R. J. Bingham, *Corros. Sci.*, **33**, 799 (1992).
31. R. J. Bingham, *Corrosion*, **49**, 386 (1993).
32. B. Wu, J. R. Scully, J. L. Hudson, and A. S. Mikhailov, *J. Electrochem. Soc.*, **144**, 1614 (1997).
33. T. T. Lunt, S. T. Pride, J. R. Scully, J. L. Hudson, and A. S. Mikhailov, *J. Electrochem. Soc.*, **144**, 1620 (1997).